JACS
JOURNAL OF THE AMERICAN CHEMICAL SOCIETY
Article
pubs.acs.org/JACS

An Interface Coassembly in Biliquid Phase: Toward Core–Shell Magnetic Mesoporous Silica Microspheres with Tunable Pore Size

Qin Yue,[†] Jialuo Li,[†] Wei Luo,[‡] Yu Zhang,[†] Ahmed A. Elzatahry,[∥,§] Xiqing Wang,[†] Chun Wang,[†] Wei Li,[†] Xiaowei Cheng,[†] Abdulaziz Alghamdi,[§] Aboubakr M. Abdullah,[⊥] Yonghui Deng,*[,†] and Dongyuan Zhao[†]

[†]Department of Chemistry, State Key Laboratory of Molecular Engineering of Polymers, and Shanghai Key Laboratory of Molecular Catalysis and Innovative Materials, State Key Laboratory of ASIC & System, Collaborative Innovation Center of Chemistry for Energy Materials, Fudan University, Shanghai 200433, P. R. China

[‡]State Key Laboratory for Modification of Chemical Fibers and Polymer Materials, College of Materials Science and Engineering, Donghua University, Shanghai 201620, P. R. China

[∥]Materials Science and Technology Program, College of Arts and Sciences, Qatar University, PO Box 2713, Doha 2713, Qatar

[§]Department of Chemistry, College of Science, King Saud University, Riyadh 11451, Saudi Arabia

[⊥]Center for Advanced Materials, Qatar University, Doha 2713, Qatar

Supporting Information

ABSTRACT: Core–shell magnetic mesoporous silica microspheres (Magn-MSMs) with tunable large mesopores in the shell are highly desired in biocatalysis, magnetic bioseparation, and enrichment. In this study, a shearing assisted interface coassembly in *n*-hexane/water biliquid systems is developed to synthesize uniform Magn-MSMs with magnetic core and mesoporous silica shell for an efficient size-selective biocatalysis. The synthesis features the rational control over the electrostatic interaction among cationic surfactant molecules, silicate oligomers, and Fe_3O_4@RF microspheres (RF: resorcinol formaldehyde) in the presence of shearing-regulated solubilization of *n*-hexane in surfactant micelles. Through this multicomponent interface coassembly, surfactant-silica mesostructured composite has been uniformly deposited on the Fe_3O_4@RF microspheres, and core–shell Magn-MSMs are obtained after removing the surfactant and *n*-hexane. The obtained Magn-MSMs possess excellent water dispersibility, uniform diameter (600 nm), large and tunable perpendicular mesopores (5.0–9.0 nm), high surface area (498–623 m^2/g), large pore volume (0.91–0.98 cm^3/g), and high magnetization (34.5–37.1 emu/g). By utilization of their large and open mesopores, Magn-MSMs with a pore size of about 9.0 nm have been demonstrated to be able to immobilize a large bioenzyme (trypsin with size of 4.0 nm) with a high loading capacity of ~97 μg/mg via chemically binding. Magn-MSMs with immobilized trypsin exhibit an excellent convenient and size selective enzymolysis of low molecular proteins in the mixture of proteins of different sizes and a good recycling performance by using the magnetic separability of the microspheres.

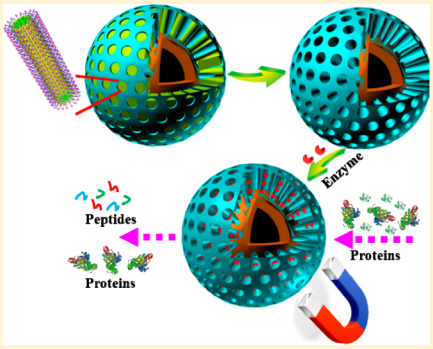

INTRODUCTION

Ordered mesoporous materials, since their discovery,[1−3] have appealed an increasing attention for their potential applications in adsorption,[4,5] catalysis,[6,7] drug delivery,[8,9] and sensors.[10] Particularly, ordered mesoporous silica materials have been considered to be ideal enzyme immobilization supports for their excellent properties including high surface area, uniform mesopores, large pore volume, various mesostructures, and biocompatibility.[11,12] On the other hand, magnetic nanomaterials have recently attracted numerous researchers' interest in catalysis, adsorption, and enrichment due to their convenient manipulation, such as magnetic separation and recycling.[13−18] Therefore, great efforts have been devoted to integrate magnetic component with mesoporous silica materials for various bioapplications.[19−31] Min et al. synthesized magnetically separable Fe_3O_4-SBA-15 hybrid materials by electrostatic depositing magnetic nanoparticles onto mesoporous silica (SBA-15) particles with a pore size of 6.0 nm;[19] however, the uncontrollable synthesis process gave rise to hybrid materials with poor morphology and blocked mesopore channels, which was disadvantageous to enzyme immobilization. Core–shell magnetic mesoporous spheres comprising magnetic core and mesoporous shell with relatively larger mesopores (>4 nm at least) are supposed to be an ideal candidate for enzyme immobilization in proteolysis, because the spheres have a good dispersibility in solution, a short diffusion distance of mass transport. Most of previous reports about magnetic mesoporous silica microspheres (abbreviated as Magn-MSMs) were synthesized by using small cationic surfactant (cytyltrimethlyammonium boromide, CTAB) as a pore forming agent, which led to the pore size less than 2.5 nm.[23−27] Such small mesopores are not suitable for enzyme immobilization for

Received: May 31, 2015
Published: July 17, 2015

DOI: 10.1021/jacs.5b05619
J. Am. Chem. Soc. 2015, 137, 13282–13289

proteolysis, because most proteins have a hydrodynamic diameter of larger than 3.2 nm and thus they can not enter into the pore channels to interact with the immobilized enzyme.[32] Although an attempt has recently been made by employing high-molecular weight copolymers to produce larger mesopores, the resultant mesoporous silica shell on magnetic particles have circular pore channels with a diameter of 4.5 nm which are difficult to access for proteins.[33] Therefore, it is of great importance and interest to develop new methods to controllably grow a mesoporous shell with a large and easily accessible mesopore on magnetic particles, so as to meet the requirements in various biorelated applications, such as immobilization of enzyme, loading precious metal nanoparticles, and so forth.

Herein, in this work, we demonstrate a shearing assisted interface coassembly in biliquid phase systems to synthesize highly dispersed Magn-MSMs with well-defined core−shell structure, large and radially aligned mesopores. This method is achieved by the coassembly of CTAB template molecules and silica oligomers on the presynthesized resorcinol formaldehyde (RF) resin coated magnetite particles (Fe_3O_4@RF) in the *n*-hexane/water biliquid phase system. In this well-designed system, tetraethyl orthosilicate dissolved in *n*-hexane phase can be hydrolyzed in the oil−water interface and invade into the water phase containing ammonia−water, CTAB, and Fe_3O_4@RF and coassemble with surfactant CTAB on the Fe_3O_4@RF microspheres. Through changing the shearing force strength in the early stage of the synthesis, the distribution of *n*-hexane in water can be tuned with help of CTAB micelles. Thus, after removing template molecules, Magn-MSMs with excellent water dispersibility, uniform sizes (~600 nm), and tunable perpendicular mesopores of 5.0−9.0 nm, high surface area (498−623 m^2/g), large pore volume (0.91−0.98 cm^3/g), and high magnetization (34.5−37.1 emu/g) were obtained. Trypsin, with a molecular size of about 4 nm, was loaded into the Magn-MSMs mesopores with a loading capacity of 97 μg/mg via chemical binding, which exhibits an excellent enzymolysis size selectivity for low molecular proteins and good recycling stability assisted by the convenient magnetic separation.

EXPERIMENTAL SECTION

Chemicals. $FeCl_3 \cdot 6H_2O$, trisodium citrate, sodium acetate, tetraethyl orthosilicate (TEOS), resorcinol, formaldehyde, ethanol, ethylene glycol, hexane, and concentrated ammonia solution (28 wt %) are of analytical grade (Shanghai Chemical Corp.). Cetyltrimethylammonium bromide (CTAB) and 3-glycidoxypropyltrimethoxysilane (GLYMO) was supplied by Sigma-Aldrich. For enzymolysis, tosylphenylalanylchloromethylketone (TPCK)-treated trypsin, bovine serum albumin (BSA), lysozyme, cytochrome *c* (Cyt-c), and myoglobin were purchased from Sigma Chemical (St. Louis, MO). Water was purified using a Milli Q system (Millipore, Molsheim, France). All other chemicals were used as received.

Synthesis of Fe_3O_4@RF Microspheres. Magnetite Fe_3O_4 particles with a mean diameter of ~200 nm were synthesized as previously described.[34] An amount of 100 mg of Fe_3O_4 particles was dispersed in a mixture solution of ethanol (20 mL) and deionized water (10 mL) by ultrasonication. Into the resultant dispersion, concentrated ammonia solution (0.5 g, 28 wt %), resorcinol (0.1 g, 0.09 mM), and formaldehyde (0.1 g, 37 wt %) were added consecutively, and the mixed dispersion was mechanically stirred for 2 h at 30 °C. After polymerization, the magnetite Fe_3O_4 particles could be uniformly coated by a layer of RF resin, and the obtained core−shell Fe_3O_4@RF microspheres were collected by a magnet and washed with deionized water and ethanol three times, respectively.

Synthesis of Fe_3O_4@RF@Mesoporous Silica Microspheres. In a typical synthesis, the Fe_3O_4@RF microspheres (0.12 mg) were redispersed in a mixed solution containing CTAB (0.5 g, 1.3 mmol), deionized water (80 mL, the concentration of CTAB was 17 mmol/L, higher than its critical micelle concentration of 0.8 mmol/L), and concentrated ammonia solution (0.8 mL, 28 wt %) with ultrasonication treatment. Into the water solution, 20 mL of *n*-hexane was added to form a biliquid phase system. To tune the mesopore size and morphology, the solution was first mechanically stirred at different stirring rate (170−500 rpm) for 10 min. Subsequently, 2.5 mL of TEOS was added dropwise into the solution in 10 min, and all the syntheses were carried out under a gentle stirring rate of 170 rpm for maintaining a biliquid phase solution. After reaction for 12 h at 30 °C, the product was collected with a magnet and washed with ethanol and water. Finally, the microspheres were redispersed in 60 mL of acetone and refluxed at 70 °C for 12 h to remove CTAB templates. The extraction was repeated two times and then thoroughly washed with ethanol. Notably, in this synthesis, it was found that the stirring rate before adding TEOS influences the porous structure of the samples. Therefore, for convenience, the obtained Fe_3O_4@RF@$mSiO_2$ microspheres were denoted as Magn-MSMs-Rs (Rs stands for the prestirring rate before adding TEOS). The obtained sample was finally dried in vacuum at 40 °C for 12 h for further use.

Immobilization of Enzyme. In this study, trypsin was used as the enzyme for biocatalysis. Prior to enzyme immobilization, the Magn-MSMs were modified with GLYMO. Typically, 0.5 g of Magn-MSMs-250 microspheres was dispersed in 50 mL of toluene containing 1.0 g of GLYMO. The mixture was stirred at 30 °C for 1 h and then heated at 65 °C for 6 h. The resultant Magn-MSMs-GLYMO spheres were washed with ethanol six times and vacuum-dried overnight for further use in enzyme immobilization as follows. An amount of 5.0 mg of GLYMO-modified microspheres was dispersed in 500 μL of 1.0 g/L trypsin solution (25 mM NH_3HCO_3 as the buffer, pH ~ 8) in an Eppendorf tube. The suspension was agitated at 37 °C for 2 h. After reaction, the supernatant solution was removed with the help of a magnet. The retained magnetic microspheres were washed with deioned water three times and redispersed in 500 μL of 25 mM NH_3HCO_3 solution. The obtained sample was denoted as Magn-MSMs-trypsin.

Protein Digestion. To evaluate the size selectivity proteolysis performance of the supported enzyme, myoglobin (MW = 17 000 Da, 2.1 × 3.5 × 4.4 nm^3), lysozyme (MW = 14 388 Da, 1.9 × 2.5 × 4.3 nm^3), and Cyt-c (MW = 12 384 Da, 2.6 × 3.2 × 3.3 nm^3) were chosen as low molecular weight model proteins. Typically, these proteins were dissolved in 25 mM NH_4HCO_3 (pH = 8.0) buffer solution with a concentration of 0.5 nmol/μL, respectively. For fairness of protein digestion, equal concentrations of BSA (MW = 66 400 Da, size =5.0 × 7.0 × 7.0 nm^3) buffer solution were used as the high molecular weight model protein. The suspension of Magn-MSMs-trypsin (0.01 mg/mL, 25 mM NH_4HCO_3 as a buffer) was transferred to the mixture containing BSA and small proteins with the same concentration (0.1 nmol/μL, 25 mM NH_4HCO_3 as a buffer). The mixture was then incubated in a shaker at 37 °C for 0.5 h. For comparison, equivalent free trypsin was used for protein digestion under the same incubating conditions. Using a magnet, Magn-MSMs-trypsin was separated from the mixture and the supernatant was submitted to matrix-assisted laser desorption/ionization time of flight mass spectrometry (MALDI-TOF MS) analysis.

MALDI-TOF MS Analysis and Database Searching. The supernatant solutions mentioned above were deposited on the MALDI target using the dried droplet method. Typically, 0.4 μL of solution was spotted onto the MALDI plate and then 0.4 μL of CHCA matrix solution (5 mg/mL, 0.1% TFA in 50% ACN/H2O solution) was introduced. Positive ion MALDI-TOF MS spectra were acquired on a 4700 Proteomics Analyzer (Applied Biosystems). The sample was excited using an Nd:YAG laser (355 nm) operated at a repetition rate of 200 Hz and acceleration voltage of 20 kV. Before identifying the samples, the MS instrument was calibrated by an internal calibration mode with tryptic peptides of myoglobin.

All spectra were taken from signal-averaging of 800 laser shots with the laser intensity kept at a proper constant. GPS Explorer software (Applied Biosystems) with Mascot (Matrix Sciences, London, U.K.) as a search engine and NCBI (version of 070316) as a database were used

DOI: 10.1021/jacs.5b05619
J. Am. Chem. Soc. 2015, 137, 13282−13289

to identify proteins. Standard proteins were identified with peptide fingerprint mass spectra. The peptide mass tolerance was set to 100 ppm, and the tandem mass tolerance was set to 0.8 Da.

Measurements and Characterization. Transmission electron microscopy (TEM) experiments were conducted on a JEOL 2011 microscope (Japan) operated at 200 kV. To investigate the interior structures of mesoporous silica shells, the samples were embedded in a white resin and cut with ultramicrotome to thin sections with a thickness below 100 nm. Field-emission scanning electron microscopy (FESEM) images were collected on the Hitachi Model S-4800 field emission scanning electron microscope (Japan). Scanning electron microscopy (SEM) images were collected with Philips XL30 electron microscope (Holland) operated at 20 kV. A thin gold film was sputtered on the samples before SEM measurements. Powder X-ray diffraction (XRD) patterns were recorded on a Bruker D4 X-ray diffractometer (Germany) with Ni-filtered Cu KR radiation (40 kV, 40 mA). Nitrogen sorption isotherms were measured at 77 K with a Micromeritcs Tristar 3000 analyzer. Before measurements, the samples were degassed in a vacuum at 100 °C for 10 h. The Brunauer–Emmett–Teller (BET) method was utilized to calculate the specific surface areas (S_{BET}) using adsorption data in a relative pressure range from 0.005 to 0.25. By using the Barrett–Joyner–Halenda (BJH) model, the pore volumes and pore size distributions were derived from the adsorption branches of isotherms, and the total pore volumes (V_t) were estimated from the adsorbed amount at a relative pressure P/P_0 of 0.995.

RESULTS AND DISCUSSION

Synthesis and Characterization. The overall synthesis procedure of Magn-MSMs and enzyme immobilization are depicted in Scheme 1A. First, water dispersible Fe_3O_4 particles were coated with a protective shell of RF resin through interface sol–gel polymerization of resorcinol and formaldehyde. Then, a layer of organic solvent-swelled CTAB/silica mesostructured composites were further deposited on the surface of the RF shells through an interface coassembly in the *n*-hexane/aqueous solution biliquid systems using TEOS as a silica precursor and CTAB as a structure-directing agent under stirring rate of 170 rpm. Third, the organic solvent and CTAB were removed by acetone extraction. Fourth, the obtained Magn-MSMs were further modified with 3-glycidoxy-propyltrimethoxysilane (GLYMO) in toluene. Finally, trypsin, a spherical enzyme of about 4.0 nm in size,[35] was immobilized in the mesopores through reaction of the amino acid groups of the enzyme and the epoxy groups of GLYMO anchored on the pore walls of mesoporous silica shells. The obtained Magn-MSMs with trypsin immobilized in mesopores were denoted as Magn-MSMs-trypsin.

The water dispersible Fe_3O_4 particles made of numerous nanosized nanoparticles were synthesized through the well-established solvothermal method.[34] SEM image shows that magnetite Fe_3O_4 particles are uniform in both morphology and size (Supporting Information Figure S1a). The TEM image reveals that the as-synthesized Fe_3O_4 particles consist of magnetite nanocrystals and have a mean diameter of 200 nm (Figure 1a). This unique structure of the magnetite particle helps to achieve a fast magnetic separation process because the Brownian motion of magnetic particles can be suppressed with an applied magnetic field; meanwhile, it prevents the irreversible aggregation of magnetic particles after removal of magnetic field, because every large particle is made of magnetite nanocrystals which are superparamagnetic. Due to the strong complexation between iron ions and phenolic hydroxyl groups,[36] resorcinol molecules can attach onto the surface of Fe_3O_4 particles and in situ polymerize with formaldehyde to form a shell of RF resin in the basic solution. SEM observations indicate that the resultant Fe_3O_4@RF microspheres have very uniform size of about 420 nm and regularly spherical morphology (Figure S1b). TEM observations indicate a distinct core–shell structure with a shell RF thickness of 100 nm (Figure 1b). Using the Fe_3O_4@RF microspheres as seeds, a shell of mesoporous silica was formed

Scheme 1[a]

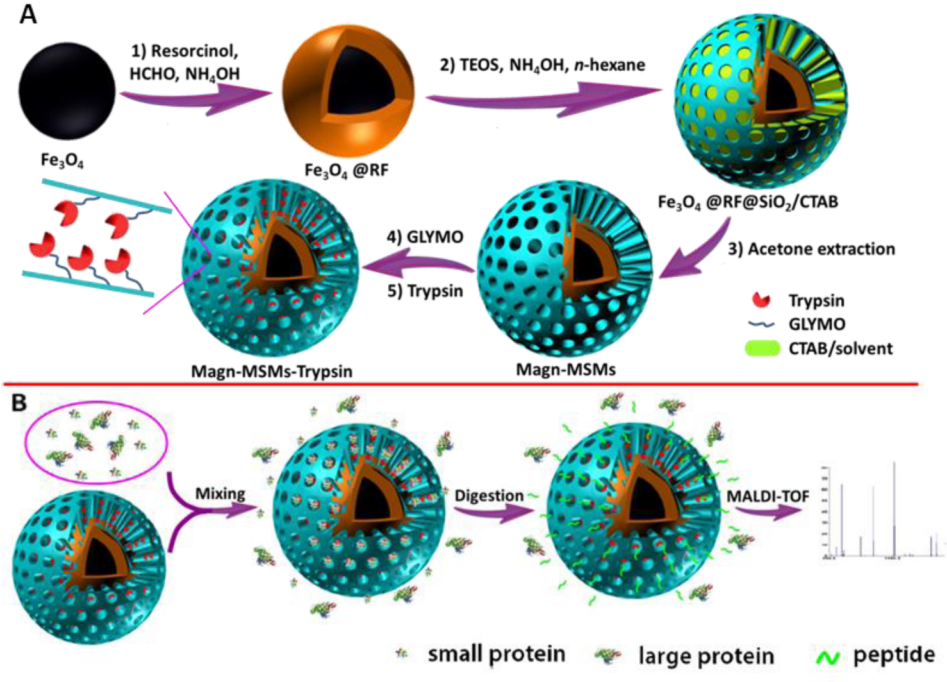

[a](A) Synthesis procedure for the Magn-MSMs and immobilization of trypsin. (B) Application of Magn-MSMs-trypsin for protein digestion. Step 1, incubation of the immobilized trypsin in mixed proteins; step 2, protein digestion; step 3, the detection of peptides by MALDI-TOF.

DOI: 10.1021/jacs.5b05619
J. Am. Chem. Soc. 2015, 137, 13282–13289

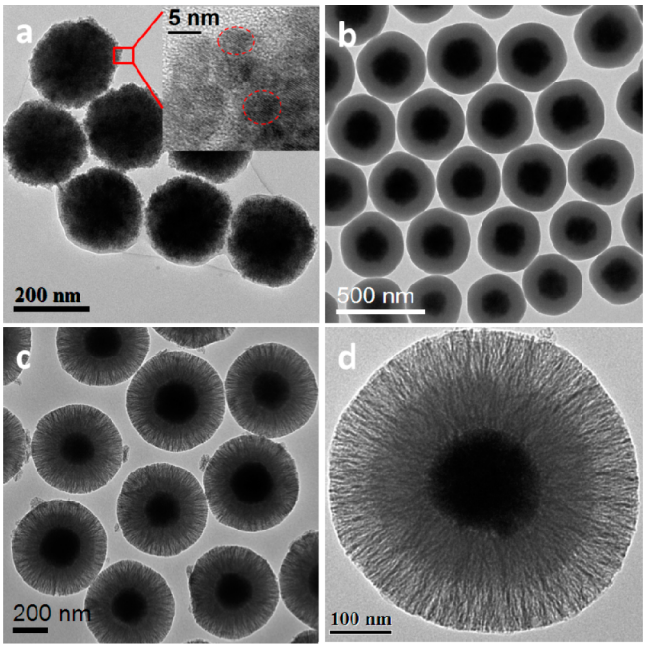

Figure 1. TEM images of (a) Fe_3O_4 particles, (b) Fe_3O_4@RF microspheres, and (c, d) Magn-MSMs-170. Inset in (a) is the enlarged high-resolution TEM image of the Fe_3O_4 particle.

on the microspheres through the coassembly of CTAB and silicate oligomers derivated from the hydrolysis of TEOS in the basic solution and the subsequent removal of CTAB templates through extraction using acetone. The obtained core−shell−shell Fe_3O_4@RF@mSiO_2 (Magn-MSMs-170) exhibits uniform spherical morphology without aggregation (Figure S2a). TEM images (Figure 1c, d) exhibit distinct core−shell−shell structure with the outer shell comprising radially aligned mesopore channels. The porous silica shells are about 90 nm in thickness from the TEM image (Figure 1d). Notably, in this study, the mesoporous silica shell thickness can be tuned from 20 to 200 nm by simply changing the feeding amount of the silica source.

N_2 adsorption−desorption isotherm of Magn-MSMs-170 microspheres (Figure 2) shows representative type-IIb curves

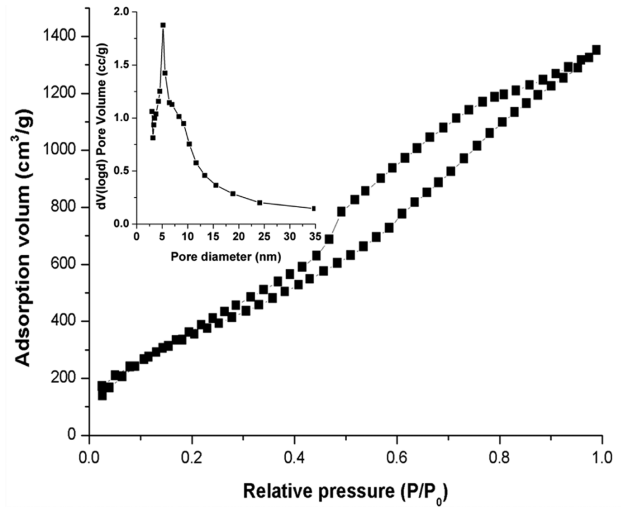

Figure 2. Nitrogen adsorption−desorption isotherms (a) and pore size distribution profile (b) of Magn-MSMs-170 microspheres synthesized in the *n*-hexane/water biliquid phase with a prestirring rate of 170 rpm.

according to the theory proposed by Rouquerol et al.,[37] which may result from the slightly distorted mesopores channels and the heterogeneity in adsorbent−adsorbate interactions. The pore size distribution curve (Figure 2, inset) derived from the adsorption branch reveals that the sample has a mesopore size of 5.0 nm, much larger than that (usually ∼2.2 nm) of conventional mesoporous materials obtained by simply using CTAB as the template.[23−27] The BET surface area and total pore volume of Magn-MSMs-170 microspheres were calculated to be ∼623 m^2/g and 0.91 cm^3/g, respectively. The wide-angle XRD patterns (Figure S3) show the typical characteristic diffraction peaks assigned to magnetite phase, indicating that the magnetite component in the composite is well retained in the whole synthesis process. Magnetic property characterization (Figure S4) using a superconducting quantum interference device at 300 K reveals that Magn-MSMS-170 microspheres have a high magnetization saturation value of 34.5 emu/g, which favors a fast separation process. Additionally, no remanence was detected, reflecting an intrinsic superparamagnetic property due to the presence of nanosized magnetite in the core of Magn-MSMs-170 microspheres.

By tuning the stirring rate during the biliquid interface coassembly synthesis, the mesopore size of Magn-MSMs can be readily tuned. As the prestirring rate (R_s) increases from 170, to 250, and to 500 rpm, the Magn-MSMs-250 and Magn-MSMs-500 synthesized with a stirring rate of 250 and 500 rpm possess regular spherical morphology, but their surface becomes rougher (Figure S2b, c), and even large holes of about 50 nm can be clearly observed in Magn-MSMs-500 surface (Figure S2c). TEM images of Magn-MSMs-250 and Magn-MSMs-500 show similar sandwich structure and obviously larger mesopores as compared with Magn-MSMs-170 (Figure 3). N_2 adsorption−desorption

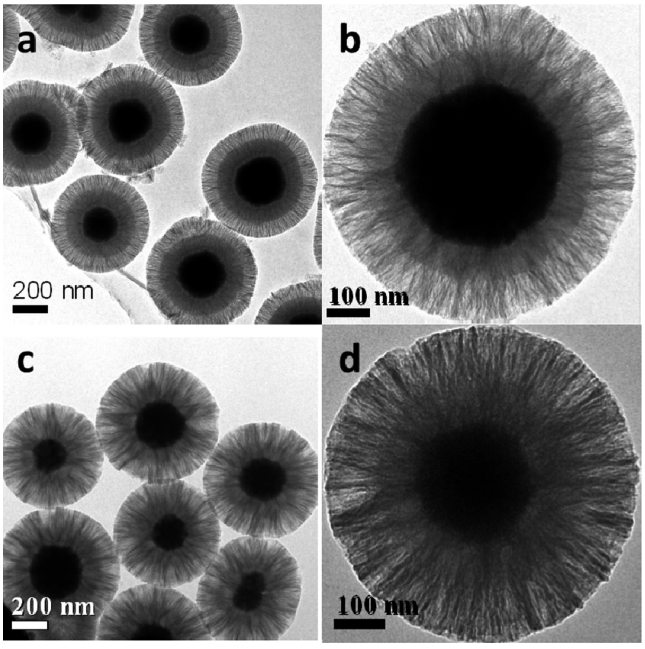

Figure 3. TEM images of Magn-MSMs-250 (a, b) and Magn-MSMs-500 (c, d) microspheres.

measurements (Figure S5a) reveal that Magn-MSMs-250 and Magn-MSMs-500 have type IV and type IIb curves, respectively. The pore size distribution profiles (Figure S5b) show that Magn-MSMs-250 has a relatively uniform pore size of 9.0 nm,

DOI: 10.1021/jacs.5b05619
J. Am. Chem. Soc. 2015, 137, 13282−13289

larger than that of Magn-MSMs-170 (5.0 nm), and Magn-MSMs-500 has two sets of mesopores located at 8.8 and 18.8 nm, respectively. It suggests that the increase of prestirring rate helps to expand the mesopores size, but too fast stirring can cause an inhomogeneous pore expansion. To further gain information about the interior structure of the samples, the Magn-MSMs sample was sliced for TEM observation. The magnetic core and radially aligned mesopores with a uniform size can be clearly visible in the sliced Magn-MSMs-170 (Figure S6a). While in the sliced Magn-MSMs-500, in addition to radial mesopores of about 9.0 nm, some larger mesopores of about 30−40 nm can be observed (Figure S6b), in good agreement with the SEM images (Figure S2c). Table 1 shows that the samples with a larger mesopore have lower surface areas and larger pore volumes. They all have high saturation magnetization values of ∼36 emu/g, which is favorable for a fast magnetic response for practical magnetic separation applications. It is worth noting that, since the RF interlayer can be removed by combustion in air, such a core−shell−shell structure can be easily converted into a unique yolk−shell structure with magnetic core trapped in a hollow mesoporous silica microsphere via calcination treatment in air at 500 °C for 5 h (Figure S7).

Table 1. Texture Properties and Magnetic Property of the Obtained Magn-MSMs

samples	BET surface area (m^2/g)[a]	total pore volume (cm^3/g)[b]	pore size (nm)[c]	magnetization (emu/g)
Magn-MSMs-170	623	0.91	5.0	34.5
Magn-MSMs-250	507	0.98	9.0	36.8
Magn-MSMs-500	498	0.96	8.8, 18.8	37.1

[a]The BET specific surface areas were calculated using adsorption data in P/P_0 range of 0.05−0.25. [b]The total pore volumes were estimated based on the volume adsorbed at $P/P_0 \sim 0.995$. [c]The pore sizes were derived from the adsorption branches of the isotherms by using the BJH method.

Formation Mechanism. The above-mentioned results clearly indicate that the evolution of the morphology and pore size of Magn-MSMs has direct relationship with the prestirring rate. To gain insight about the influence of stirring rate, we prepared a biliquid system of CTAB-ammonia−water−Fe_3O_4@RF/*n*-hexane. The system was stirred at 170, 250, and 500 rpm, respectively, and subsequently, a small amount of water solution was withdrawn for dynamic light scattering (DLS) measurements at 25 °C. According to the DLS results, micelles have a relatively uniform size of about 6.0 nm at 170 rpm (Figure S8a), and when the prestirring (prior to adding TEOS) rate is increased to 250 rpm, most of the micelle size increases to ∼20.2 nm (Figure S8b), although small amount of micelles remain the size of about 6.0 nm. With a fast stirring of 500 rpm, most micelles achieve a size of about 20.0 nm; meanwhile some larger micelles of about 70.0 nm (Figure S8c) are present due to the solubilization of CTAB micelles enhanced by the dynamic shearing force of high-speed stirring.

Based on the above results, we proposed a shearing assisted biliquid interface coassembly mechanism for the formation of core−shell−shell magnetic mesoporous silica microspheres (Magn-MSMs). As depicted in Figure 4, at the beginning, a two-phase system is formed by adding hydrophobic *n*-hexane into the aqueous solution containing CTAB surfactant, Fe_3O_4@RF microspheres, and ammonia−water. Then, under mild mechanical stirring at 170−500 rpm, *n*-hexane can be continuously absorbed by the preformed CTAB micelles due to the strong hydrophobic interaction between CTAB and *n*-hexane molecule, which is related with the "like dissolves like" principle. Also the well-matched chain length of CTAB and *n*-hexane helps to stabilize the composite micelles,[38,39] although the distribution of *n*-hexane in CTAB micelles varies dynamically between the water and *n*-hexane bulk phase during the continuous stirring. The size of the expanded composite micelles is related with the shearing force of the mechanical stirring. After that, upon the addition of TEOS into *n*-hexane phase, oligomer silicate nanoclusters could be generated at the oil/water interface through hydrolysis and condensation of TEOS catalyzed by ammonia−water. They further associate with CTAB micelles through electrostatic interaction, coassemble into rodlike *n*-hexane-CTAB-silica composite micelles with different sizes, and deposit on Fe_3O_4@RF microspheres through a radial alignment due to the electrostatic interaction between the composite micelles and hydrophilic RF shell and the lowest interface energy requirement.[23,40] After the structure of the composite is fixed with a cross-linked silica framework, CTAB and *n*-hexane can be completely removed through acetone treatment, resulting in core−shell−shell magnetic mesoporous

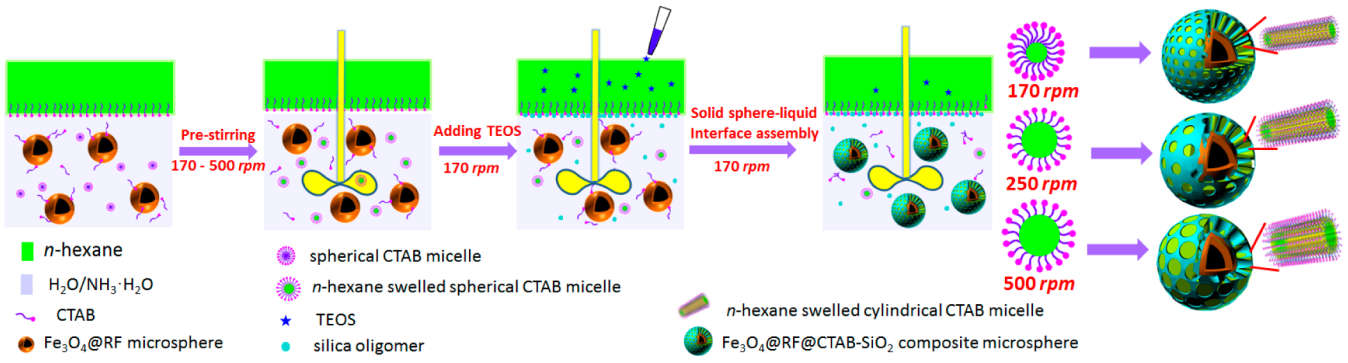

Figure 4. Schematic illustration of the formation process for Magn-MSMs with tunable mesopore size via the biliquid interface coassembly. In the biliquid system, the water phase consists of water, Fe_3O_4@RF microspheres, basic catalyst, and spherical CTAB micelles. Before adding TEOS, the prestirring at different speeds of 170−500 rpm leads to CTAB micelles of different sizes as a result of the continuous dynamic solubilization of *n*-hexane in CTAB micelles. After introduction of TEOS, the generated negatively charged silica oligomers interact with the micelles in water, coassemble into rodlike composite micelles with different sizes, deposit on the interface of Fe_3O_4@RF microspheres through a radial alignment due to the electrostatic interaction and the lowest interface energy requirement, and finally fix the mesostructure on Fe_3O_4@RF microspheres. Thus, after removing CTAB and *n*-hexane, Magn-MSMs with mesoporous silica shell of different pore sizes can be generated.

DOI: 10.1021/jacs.5b05619
J. Am. Chem. Soc. 2015, 137, 13282−13289

silica microspheres with different mesopores size. In the whole synthesis, *n*-hexane serves as the oilphase to expand the micelle sizes through dynamically swelling CTAB micelles.

Immobilization of Trypsin for Size Exclusion Proteolysis. Proteolysis is an important biocatalysis process, which is a useful pathway to acquire information on proteins in proteome analysis.[41,42] The low molecular-weight (MW) proteomes have aroused great interest in understanding pathological and biomedical systems for their potential application in the biomarkers and signal molecules.[43] However, the low MW proteome determinations are considered to be a great challenge due to the interference of abundant high MW proteomes.[44,45] Here, in this study, we investigated the feasibility to solve these problems by using our Magn-MSMs that possess two important merits, that is, the large and tunable pore sizes for immobilization of enzyme for possible size-selective protein digestion, and the convenient magnetic separation. Enzyme immobilization helps to increase the stability and activity of enzyme due to avoidance of protein self-enzymolysis, unfolding and aggregation after immobilized on solid supports.[46−49] Traditional core−shell structural magnetic mesoporous silica particles possess mesopores of 2 nm in diameter, which is too small for immobilization of enzyme into the pores. Our magnetic mesoporous silica microspheres with well-controlled mesopores of 5.0−9.0 nm can be served as an ideal enzyme supports (Scheme 1b). Trypsin, a spherical enzyme with size of 3.8 × 3.8 × 3.8 nm^3, was chosen to immobilize into the mesopores of Magn-MSMs-250. Before immobilization, GLYMO was used as a linker for trypsin due to the strong interaction of epoxy group of GLYMO with functional group in amino acid residues of trypsin. Through simple aqueous reaction, trypsin could be immobilized into the mesopores of Magn-MSMs-250 within 1 h, which was confirmed by the UV absorption value of the supernatant trypsin after the immobilization procedure. The immobilization capability of Magn-MSMs-250 for trypsin can reach 97 μg/mg (enzyme/supports), higher than most of the reported results based on mesoporous silica.[50] Fourier transform infrared (FTIR) spectra (Figure S9) of Magn-MSMs-250 after immobilizing trypsin exhibit new characteristic absorption bands in the range of 1200−1600 cm^{-1}, further confirming a successful immobilization.

Trypsin immobilized Magn-MSMs-250 (denoted as Magn-MSMs-trypsin) was used for the size exclusion proteolysis. Several small proteins with different molecular weight and size including myoglobin, lysozyme, and Cyt-c[49] mixed with a large protein BSA, respectively, were tested for size exclusion proteolysis by using Magn-MSMs-trypsin with the mesopore size of 9.0 nm in diameter. For comparison, these protein pairs with the same concentration of 0.5 g/L were also digested using equal free trypsin in aqueous solution for 2 h. The peptides digested from these proteins were easily separated with a magnet and detected by MALDI-TOF mass spectrometry. Peptides digested from myoglobin and BSA were both detected by the MALDI-TOF using free trypsin digestion in solution (Figure 5a). However, by using Magn-MSMs-trypsin, only a small amount of peptide from BSA was detected and a dramatically increased amount of peptides from myoglobin was detected. It implies that trypsin immobilized in Magn-MSMs is accessible for myoglobin and inaccessible for BSA, demonstrating an efficient size exclusion proteolysis. The sequence coverage of BSA and myoglobin by free trypsin digestion turn out 30% and 18%, respectively. While using immobilized trypsin on Magn-MSMs to digest the proteins, the sequence coverages of 5% for BSA and 33% for myoglobin were obtained, reflecting obvious superiority digestion efficiency

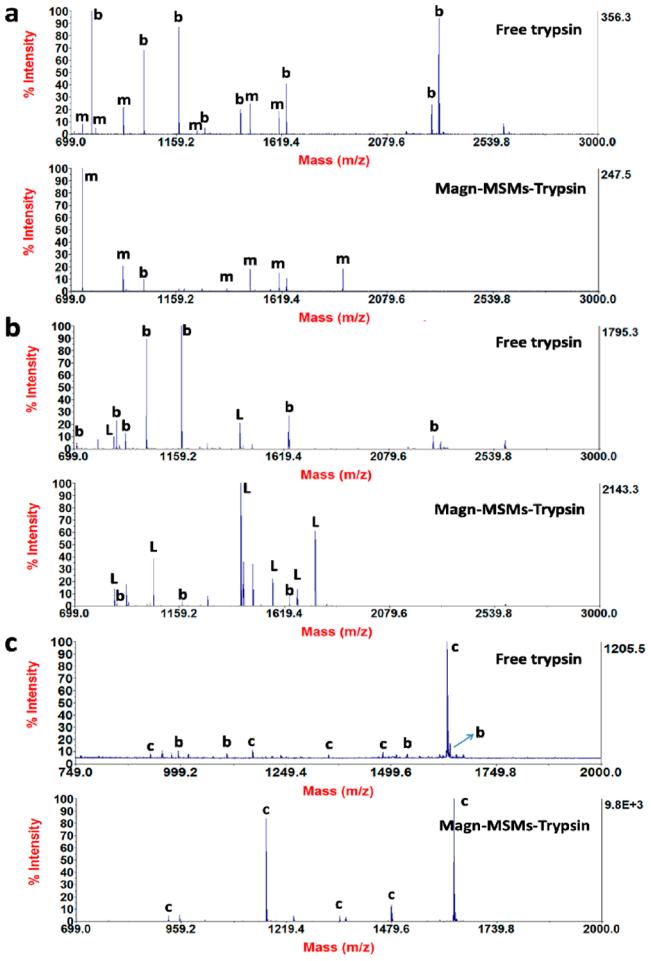

Figure 5. MALDI-TOF spectra of tryptic digests of (a) myoglobin, (b) lysozyme, and (c) Cyt-c mixed with BSA after being treated by trypsin immobilized on Magn-MSMs microspheres and free trypsin at 37 °C for 2 h. The peptide peaks at relatively high S/N are labeled with m, L, c, and b which are assigned to peptides derived from myoglobin, lysozyme, Cyt-c, and BSA, respectively.

for small protein. In the case of lysozyme−BSA mixture (Figure 5b), using free trypsin for digestion, abundant BSA peptide fragments were detected. In contrast, Magn-MSMs-trypsin digested peptides are almost from lysozyme. The sequence coverage (Figure S10) of BSA decreased from 40% to 9% while that of lysozyme increased from 27% to 46% by Magn-MSMs-trypsin digestion, further indicating the size-independent digestion. Besides, Magn-MSMs-trypsin also represents priority digestion for small protein Cyt-c than for large BSA (Figure 5c). All these results show that Magn-MSMs-trypsin can digest proteins with a small size rather than large BSA because proteins smaller than the mesopore size can easily enter into the mesopores and are in-pore digested, while large proteins are excluded outside. The magn-MSMs-trypsin can be easily recycled by using a magnet and exhibits well-retained catalytic performance after use for eight times. The recycled Magn-MSMs-trypsin after use for eight cycles possesses intact pore structure and core−shell structure (Figure S11), indicating a good structure and performance stability of this novel biocatalyst.

■ CONCLUSIONS

In summary, a shearing assisted interface coassembly in biliquid phase systems has been developed to synthesize high quality

DOI: 10.1021/jacs.5b05619
J. Am. Chem. Soc. 2015, 137, 13282−13289

core−shell magnetic mesoporous silica microspheres (Magn-MSMs) with large tunable size and open pore structure. Through the interface coassembly of CTAB molecules and silica oligomers on the Fe_3O_4@RF microspheres in *n*-hexane/water biliquid phase system, combined with mechanical stirring, highly dispersible Magn-MSMs with uniform sizes (~600 nm), large and tunable perpendicular mesopores of 5.0−9.0 nm, high surface area up to 623 m^2/g, and large pore volume of 0.9 cm^3/g can be obtained. By utilization of the unique core−shell structure, magnetic separation technique, and the designed pore size (~9.0 nm), trypsin with a molecule size of ~4.0 nm was successfully immobilized on the pore wall of Magn-MSMs with a high loading capacity of 97 μg/mg. The immobilized enzyme exhibits an excellent size selectivity enzymolysis for low molecular proteins in the mixture of proteins with different sizes and good recycling stability. Considering the simplicity and good reproducibility of the synthesis route, it is expected that the interface coassembly in a biliquid system can be extended to design other functional nanostructures with multi-components and integrated properties for various applications.

■ ASSOCIATED CONTENT

Supporting Information

SEM images of Fe_3O_4 particles, Fe_3O_4@RF microspheres, Magn-MSMs-170, Magn-MSMs-250, and Magn-MSMs-500; wide-angle X-ray diffraction patterns and magnetization hysteresis loops of Magn-MSMs-170. Nitrogen adsorption−desorption isotherms and pore size distributions of Magn-MSMs-250 and Magn-MSMs-500. TEM images of Magn-MSMs-170 and Magn-MSMs-500 after ultrathin microtomming. TEM images of the yolk−shell magnetic mesoporous silica microspheres obtained after removing the middle RF resin shell through calcination treatment of Magn-MSMs-250 and Magn-MSMs-500 at 500 °C for 5 h in air. DLS measurement results of micelles in the aqueous solutions, FTIR spectra of Magn-MSMs, trypsin, and Magn-MSMs-trypsin, sequence coverage of myoglobin, lysozyme, and Cyt-c mixed with BSA under digestion by free trypsin and immobilized trypsin on Magn-MSMs microspheres at 37 °C for 2 h. The Supporting Information is available free of charge on the ACS Publications website at DOI: 10.1021/jacs.5b05619.

■ AUTHOR INFORMATION

Corresponding Author

*yhdeng@fudan.edu.cn

Notes

The authors declare no competing financial interest.

■ ACKNOWLEDGMENTS

This work was supported by the State Key 973 Program of PRC (2013CB934104), the NSF of China (51372041, 51422202, 51402049, and 51432004), the innovation program of Shanghai Municipal Education Commission (13ZZ004), Program for New Century Excellent Talents in University (NCET-12-0123), the "Shu Guang" Project (13SG02) supported by Shanghai Municipal Education Commission and Shanghai Education Development Foundation, Shanghai Committee of Science and Technology (14ZR1400600), State Key Laboratory of ASIC & System (2015KF002), Foundation of State Key Laboratory of Pollution Control and Resource Reuse (Tongji University), China (PCRRF14017), and Qatar University startup Grant No. QUSG-CAS-MST-14\15-1. We extend our appreciation to the Deanship of Scientific Research at King Saud University for funding the work through the research group Project No. RGP-227. We thank Prof. Guangrong Zhou for help in TEM characterization.

■ REFERENCES

(1) Kresge, C. T.; Leonowicz, M. E.; Roth, W. J.; Vartuli, J. C.; Beck, J. S. *Nature* **1992**, *359*, 710.
(2) Zhao, D. Y.; Feng, J. L.; Huo, Q. S.; Melosh, N.; Fredrickson, G. H.; Chmelka, B. F.; Stucky, G. D. *Science* **1998**, *279*, 548.
(3) Che, S.; Liu, Z.; Ohsuna, T.; Sakamoto, K.; Terasaki, O.; Tatsumi, T. *Nature* **2004**, *429*, 281.
(4) Vinu, A.; Murugesan, V.; Tangermann, O.; Hartmann, M. *Chem. Mater.* **2004**, *16*, 3056.
(5) Sun, Z. K.; Deng, Y. H.; Wei, J.; Gu, D.; Tu, B.; Zhao, D. Y. *Chem. Mater.* **2011**, *23*, 2176.
(6) Wan, Y.; Zhao, D. Y. *Chem. Rev.* **2007**, *107* (7), 2821.
(7) Joo, S. H.; Choi, S. J.; Oh, I.; Kwak, J.; Liu, Z.; Terasaki, O.; Ryoo, O. R. *Nature* **2001**, *412*, 169.
(8) Kim, J.; Lee, J. E.; Lee, J.; Yu, J. H.; Kim, B. C.; An, K.; Hwang, Y.; Shin, C. H.; Park, J. G.; Kim, J.; Hyeon, T. *J. Am. Chem. Soc.* **2006**, *128*, 688.
(9) Zhang, L.; Qiao, S. Z.; Jin, Y. G.; Chen, Z. G.; Gu, H. C.; Lu, G. Q. *Adv. Mater.* **2008**, *20*, 805.
(10) Yamada, T.; Zhou, H. S.; Uchida, H.; Tomita, M.; Ueno, Y.; Ichino, T.; Honma, I.; Asai, K.; Katsube, T. *Adv. Mater.* **2002**, *14*, 812.
(11) Kim, J.; Grate, J. W.; Wang, P. *Chem. Eng. Sci.* **2006**, *61*, 1017.
(12) Fan, J.; Shui, W. Q.; Yang, P. Y.; Wang, X. Y.; Xu, Y. M.; Wang, H. H.; Chen, X.; Zhao, D. Y. *Chem. - Eur. J.* **2005**, *11*, 5391.
(13) Katz, E.; Willner, I. *Angew. Chem., Int. Ed.* **2004**, *43*, 6042.
(14) Park, J.; An, K. J.; Hwang, Y. S.; Park, J. G.; Noh, H. J.; Kim, J. Y.; Park, J. H.; Hwang, N. M.; Hyeon, T. *Nat. Mater.* **2004**, *3*, 891.
(15) Lu, A. H.; Salabas, E. L.; Schuth, F. *Angew. Chem., Int. Ed.* **2007**, *46*, 1222.
(16) Ge, J. P.; Zhang, Q.; Zhang, T. R.; Yin, Y. D. *Angew. Chem., Int. Ed.* **2008**, *47*, 8924.
(17) Zhang, L.; Qiao, S. Z.; Jin, Y. G.; Chen, Z. G.; Gu, H. C.; Lu, G. Q. *Adv. Mater.* **2008**, *20*, 805.
(18) Deng, Y. H.; Deng, C. H.; Qi, D. W.; Liu, C.; Liu, J.; Zhang, X. M.; Zhao, D. Y. *Adv. Mater.* **2009**, *21*, 1377.
(19) Min, Q. H.; Zhang, X. X.; Wu, R. A.; Zou, H. F.; Zhu, J. J. *Chem. Commun.* **2011**, *47*, 10725.
(20) Kim, J.; Kim, H. S.; Lee, N.; Kim, T.; Kim, H.; Yu, T.; Song, I. C.; Moon, W. K.; Hyeon, T. *Angew. Chem., Int. Ed.* **2008**, *47*, 8438.
(21) Kim, J.; Lee, J. E.; Lee, J.; Yu, J. H.; Kim, B. C.; An, K.; Hwang, Y.; Shin, C. H.; Park, J. G.; Kim, J.; Hyeon, T. *J. Am. Chem. Soc.* **2006**, *128*, 688.
(22) Zhao, W. R.; Chen, H. R.; Li, Y. S.; Li, L.; Lang, M. D.; Shi, J. L. *Adv. Funct. Mater.* **2008**, *18*, 2780.
(23) Deng, Y. H.; Qi, D. W.; Deng, C. H.; Zhang, X. M.; Zhao, D. Y. *J. Am. Chem. Soc.* **2008**, *130*, 28.
(24) Deng, Y. H.; Cai, Y.; Sun, Z. K.; Liu, J.; Liu, C.; Wei, J.; Li, W.; Liu, C.; Wang, Y.; Zhao, D. Y. *J. Am. Chem. Soc.* **2010**, *132*, 8466.
(25) Zhang, L.; Qiao, S. Z.; Jin, Y. G.; Chen, Z. G.; Gu, H. C.; Lu, G. Q. *Adv. Mater.* **2008**, *20*, 805.
(26) Zhao, W. R.; Gu, J. L.; Zhang, L. X.; Chen, H. R.; Shi, J. L. *J. Am. Chem. Soc.* **2005**, *127*, 8916.
(27) Kim, J.; Lee, J. E.; Lee, J.; Yu, J. H.; Kim, B. C.; An, K.; Hwang, Y.; Shin, C. H.; Park, J. G.; Kim, J.; Hyeon, T. *J. Am. Chem. Soc.* **2006**, *128*, 688.
(28) Knezevic, N. *Process. Appl. Ceram.* **2014**, *8*, 109.
(29) Yang, J. P.; Shen, D. K.; Wei, Y.; Li, W.; Zhang, F.; Kong, B.; Zhang, S. H.; Teng, W.; Fan, J. W.; Zhang, W. X.; Dou, S. X.; Zhao, D. Y. *Nano Res.* **2015**, DOI: 10.1007/s12274-015-0758-2.
(30) Liu, F.; Tian, H.; He, J. H.; Liu, H. Y. *Int. J. Nanosci.* **2012**, *11*, 1240031.
(31) Li, W.; Zhang, B. L.; Li, X. J.; Zhang, H. P.; Zhang, Q. Y. *Appl. Catal., A* **2013**, *459*, 65.

DOI: 10.1021/jacs.5b05619
J. Am. Chem. Soc. 2015, 137, 13282−13289

(32) Hudson, S.; Cooney, J.; Magner, E. *Angew. Chem., Int. Ed.* **2008**, *47*, 8582.
(33) Wang, M. H.; Sun, Z. K.; Yue, Q.; Yang, J.; Wang, X. Q.; Deng, Y. H.; Yu, C. Z.; Zhao, D. Y. *J. Am. Chem. Soc.* **2014**, *136*, 1884.
(34) Liu, J.; Sun, Z. K.; Deng, Y. H.; Zou, Y.; Li, C. Y.; Guo, X. H.; Xiong, L. Q.; Gao, Y.; Li, F. Y.; Zhao, D. Y. *Angew. Chem., Int. Ed.* **2009**, *48*, 5875.
(35) Hartmann, M. *Chem. Mater.* **2005**, *17*, 4577.
(36) Sun, Z. K.; Sun, B.; Qiao, M. H.; Wei, J.; Yue, Q.; Wang, C.; Deng, Y. H.; Kaliaguine, S.; Zhao, D. Y. *J. Am. Chem. Soc.* **2012**, *134*, 17653.
(37) Rouquerol, F.; Rouquerol, J.; Sing, K. S. W.; Llewellyn, P.; Maurin, G. *Adsorption by Powders and Porous Solids*; Academic Press: New York, 2014; pp 447−449.
(38) Wu, Y. T.; Chai, J. L.; Li, X. Q.; Yang, B.; Shang, S. C.; Lu, J. J. *J. Chem. Eng. Data* **2011**, *56*, 3089.
(39) Tokiwa, Y.; Sakamoto, H.; Takiue, T.; Aratono, M.; Matsubara, H. *J. Phys. Chem. B* **2015**, *119*, 6235.
(40) Teng, Z. G.; Zheng, G. F.; Dou, Y. Q.; Li, W.; Mou, C. Y.; Zhang, X. H.; Asiri, A. M.; Zhao, D. Y. *Angew. Chem., Int. Ed.* **2012**, *51*, 2173.
(41) Pandey, A.; Mann, M. *Nature* **2000**, *405*, 837.
(42) Domonl, B.; Aebersold, R. *Science* **2006**, *312*, 212.
(43) Anderson, N. L.; Anderson, N. G. *Mol. Cell. Proteomics* **2002**, *1*, 845.
(44) Tirumalai, R. S.; Chan, K. C.; Prieto, D. A.; Issaq, H. J.; Conrads, T. P.; Veenstra, T. D. *Mol. Cell. Proteomics* **2003**, *2*, 1096.
(45) Terracciano, R.; Gaspari, M.; Testa, F.; Pasqua, L.; Tagliaferri, P.; Cheng, M. M. C.; Nijdam, A. J.; Petricoin, E. F.; Liotta, L. A.; Cuda, G.; Ferrari, M.; Venuta, S. *Proteomics* **2006**, *6*, 3243.
(46) Klibanov, A. M. *Science* **1983**, *219*, 719.
(47) Corma, A.; Fornes, V.; Rey, F. *Adv. Mater.* **2002**, *14*, 71.
(48) Zhang, Y. H.; Liu, Y.; Kong, J. L.; Yang, P. Y.; Tang, Y.; Liu, B. H. *Small* **2006**, *2*, 1170.
(49) Zhang, Y. H.; Wang, X. Y.; Shan, W.; Wu, B. Y.; Fan, H. Z.; Yu, X. J.; Tang, Y.; Yang, P. Y. *Angew. Chem., Int. Ed.* **2005**, *44*, 615.
(50) Lin, S.; Yao, G. P.; Qi, D. W.; Li, Y.; Deng, C. H.; Yang, P. Y.; Zhang, X. M. *Anal. Chem.* **2008**, *80*, 3655.

DOI: 10.1021/jacs.5b05619
J. Am. Chem. Soc. 2015, 137, 13282−13289